In-situ investigation of laser ablation of thin films*

E. Matthias[a], J. Siegel[a], S. Petzoldt[a], M. Reichling[a], H. Skurk[a], O. Käding[a], E. Neske[b]

[a]Fachbereich Physik, Freie Universität Berlin, Arnimallee 14, D-14195 Berlin, Germany
[b]Fraunhofer-Institut für Physikalische Meßtechnik Heidenhofstrasse 8, D-79110 Freiburg i. Br., Germany

Abstract

The probe beam deflection technique, based on the mirage effect, has been applied to monitor laser processing of polymer and metal films and to measure damage thresholds of optical coatings. The technique is described and it will be shown that its sensitivity permits distinguishing between surface effects like heating and cracking, causing normal sound waves, and plasma formation outside the surface, giving rise to shockwaves. Examples are presented for single-shot ablation with 14 ns laser pulses of 248 nm wavelength. In particular, ablation studies of Ni films of varying thicknesses disclose a quantitative correlation between threshold fluences and thermal properties like heat diffusion, melting, and evaporation. In contrast, for Cr films a simple thermodynamic model fails because the films crack before melting and vaporizing.

Keywords: Coatings; Dielectrics; Laser ablation; Metals

1. Introduction

Laser ablation and laser damage of thin solid films is an area of rapidly growing interest, and the present state of understanding is documented among others in Refs. [1–5]. In general, optical absorption, thermal and structural properties of the film, and adhesion to the substrate determine the damage or ablation process. According to the film properties, the field can, somewhat arbitrarily, be grouped into ablation of polymer films, processing of metal films, and damage resistance of optical coatings. In this paper, some instructive examples of each group will be discussed. Measurements of damage thresholds of oxide coatings will be discussed in more detail in another contribution to this conference [6].

There are many ways to monitor laser ablation or surface damage. Those that measure in situ range from optical techniques (reflection, transmission, scattering), applicable under any condition as long as there is optical access, to plasma analysis and element-specific particle detection (mass analysis, time-of-flight) in vacuum. Then there is the inspection of ablated or damaged areas by microscopic techniques (optical, photothermal, reflection electron microscopy (REM), scanning tunneling microscopy (STM)) or by profilometry subsequent to irradiation. In many cases, the information obtained by the different methods is complementary. The choice of the proper analytical tool depends on the specific application, and quantities such as ablation rate per pulse, deposition rate from a plasma, damage of optical components, or studies of fundamental processes, in general require different experimental approaches.

One powerful tool for recording shock wave emission and the temporal development of the plasma outside the surface is schlieren photography [7–9]. Its one-dimensional analogue is the probe beam deflection (PBD) technique, sometimes called the mirage effect, that has been used in several laboratories for monitoring ablation [10–15]. The physical principle in both cases is light deflection by a transient gradient of refractive index, which can be caused by heat, sound, and shock waves, as well as by vapor or plasma plumes. The PBD technique is a sensitive and generally applicable tool for in-situ monitoring of the surface response of materials

to pulsed laser irradiation. Heating, cracking, evaporation, and plasma formation of strongly absorbing materials can be detected in the same manner as photodissociation of polymers and breakdown of dielectrics. It is the purpose of this paper to demonstrate the potential of the PBD method, in particular for measuring threshold and subthreshold phenomena in pulsed laserlight interactions with thin films.

2. Experimental technique

The experimental scheme for PBD measurements is displayed in Fig. 1 [15]. Light from an excimer laser (in our experiments 248 nm, 14 ns pulses) is focused onto the sample and the acoustic and/or matter wave emerging from the surface is detected by the deflection of a probing HeNe laser beam running parallel to the surface. The spatial profile of the laser beam is of good top hat shape. The incident fluence (J cm^{-2}) can be varied and is monitored for each individual pulse by a pyroelectric detector (pyro A). The reflectivity of the sample is recorded by pyro B. For transparent samples, pyro B can be arranged to measure the transmission. A charge coupled device (CCD) camera serves to provide an overall picture of the irradiated surface spot.

The distance between the surface and the center of the probing beam is adjustable, but is usually kept around 3 mm. The total light path of the HeNe laser
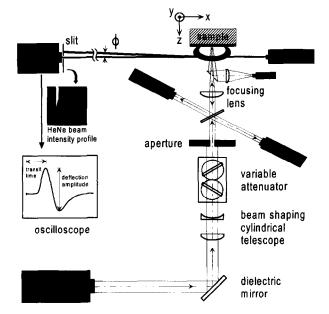
Fig. 1. Experimental scheme for monitoring ablation or surface damage by deflection of a HeNe probe beam due to a transient gradient of the refractive index. The acoustic signal utilized in the measurements is shown in the inset. Pyrodetector B can be placed as shown to detect the reflectivity or, alternatively, behind a transparent sample to monitor the transmission. The CCD camera conveys an overall picture of the sample surface during irradiation.
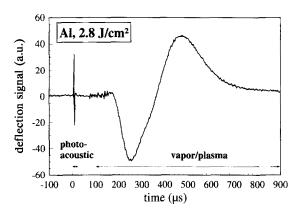
Fig. 2. Typical signal form obtained from an Al target with one single laser pulse (248 nm, 14 ns) at a fluence of 2.8 J cm^{-2}, which is above the ablation threshold. The narrow signal occuring after a few µs is of an acoustic nature due to a shock front. The bigger signal extending over several hundred µs is caused by the Al vapor plasma.

beam is 2 m, the distance between target and slit aperture about 1.5 m. This provides the necessary leverage to achieve a high sensitivity. The detection principle is indicated: the steepest slope of the HeNe laser beam profile is adjusted to the narrow slit in front of the photomultiplier in order to give the largest possible intensity variation for small deflections of the probing beam. A typical signal form, obtained with a pump laser fluence of 2.8 J cm^{-2} from an Al surface is shown in Fig. 2. It consists of a fast acoustic signal occuring after a few µs for probing beam distances of 3 mm. This signal originates either from a sonic wave, which as in photoacoustics [16] reflects the temperature of the surface, or from a shock wave generated by an expanding plasma. The acoustic signal is very reproducible and was therefore used exclusively in all experiments for gaining quantitative information. The slower and much larger signal in Fig. 2 arises from the vapor or plasma plume reaching the probing beam. Except for materials which are easy to ablate, this signal fluctuates erratically and is therefore not suitable for data evaluation. Polyimide is such an exceptional case for which it can be shown that both, the shock wave and the plasma signal are of same origin, as demonstrated in Fig. 3. Here, the peak-to-peak amplitudes of the acoustic and the plasma signals are plotted versus laser fluence. Each point represents a single shot on a virgin surface spot (1-on-1 mode). The data below 0.03 J cm^{-2} mark the noise level of the apparatus. The sudden increase of both signals at this fluence defines the threshold for ablation and is identical for both signals within an uncertainty of about 10%.

The behavior of the shock and plasma wave is further illustrated in Fig. 4, which shows the signals for ten consecutive laser pulses of 248 nm at a fluence of 0.47 J cm^{-2} on the same spot of a 400 nm Au film. The first pulse shows no response, heating and onset of vaporization can be noticed at the second pulse, and
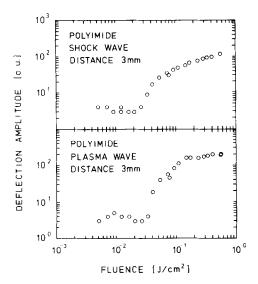
Fig. 3. Threshold behavior of polyimide for 248 nm, 14 ns laser pulses, measured with both, the shock wave signal (top) and the signal due to the plasma wave (bottom). The break of the data trend around 0.03 J cm^{-2} establishes the ablation onset.
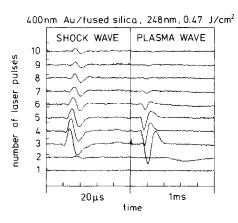

Fig. 4. Comparison of shock and plasma wave signals obtained for each consecutive laser shot on the same spot of a 400 nm Au film. Shock pulses appear between 4 and 10 μs, plasma signals around 0.2 ms. Ablation of the metal film takes place during laser pulses 3–7.
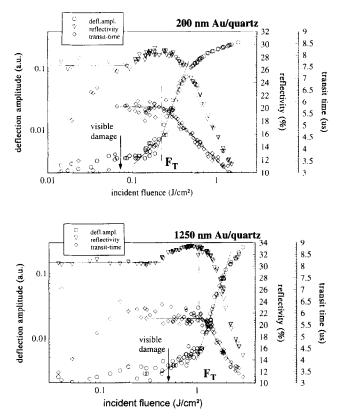

Fig. 5. Example of typical data sets measured for two Au films of different thickness on fused silica with 14 ns, 248 nm laser pulses. The arrows indicate the fluence level above which surface damage becomes visible. The dashed–dotted lines mark the fluence threshold for ablation. Solid lines are drawn to guide the eye.

ablation takes place during shot numbers 3 7. After the Au film is completely removed, the plasma signal vanishes and only an acoustic signal remains for pulses 8–10, caused by heating of the substrate surface. Note that ablation generates shock waves which arrive earlier compared with the heat signals in traces 2, 9, and 10.

Fig. 4 also demonstrates how the PBD signal can be calibrated in terms of ablation rates. Since five shots remove a 400 nm Au layer, the average ablation rate per pulse at this fluence and wavelength is 80 nm per pulse. A more precise single-shot calibration can be achieved when comparing the etch depth per pulse obtained from profilometry with the amplitude of the acoustic pulse [17]. The examples presented in this paper, however, are not concerned with absolute values of ablation rates. Instead, we are interested in investi-

gating threshold and incubation [18] characteristics, which is best done by observing the PBD signal as a function of fluence or shot number.

As defined in the inset of Fig. 1, the transit time and amplitude of the deflection signal can be measured [15]. The reflectivity of the irradiated spot is an additional piece of information. Recording all three quantities as a function of fluence leads to a typical data set shown in Fig. 5 for two different Au films. Several features can be distinguished. (1) The increase in reflectivity starts at the same fluence where microscopic imaging indicates surface damage (labeled by an arrow). We identify this fluence with the melting threshold. (2) The decrease in reflectivity coincides with a steep growth of the shock wave amplitude as well as a decrease in transit time, and signals evaporation and plasma formation. The onset is marked by a dashed–dotted line and defines the fluence threshold for ablation or damage. (3) Between arrow and ablation onset the deflection amplitude increases slowly while the transit time still remains constant. This coincides with the increase in reflectivity and signifies melting. In this range, the heated surface generates a photoacoustic sound wave [16] (compare trace 2 in Fig. 4).
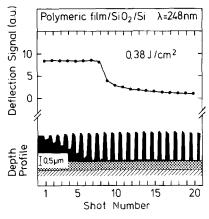
Fig. 6. Selective ablation of a photoresist film in multishot mode. Upper part, dependence of PBD amplitudes on number of laser pulses applied to the same spot; lower part, variation of the depth profile with the number of applied shots.

3. Results and discussion

3.1. Polymer films

When laser ablating thin films, there is often the requirement that the substrate or the film beneath should not be harmed. This presents no problem when the absorbance of the film material is much stronger than that of the substrate. In this case the ablation process will control itself and stop automatically at the interface. An example is displayed in Fig. 6, where the PBD amplitude is recorded as a function of laser shots on one spot (N-on-1) and compared with the etch depth for the corresponding number of pulses. The correlation between both quantities is obvious. As long as the photoresist material is ejected, the shock wave signal is large. Once the interface is reached, the PBD signal decreases abruptly, with more than a factor of 2 between shot numbers 8 and 9. The remaining small amplitude, which further decreases with increasing shot number, is due to wall ablation and vaporization of residual material left in the pit. The SiO_2 surface, however, stays intact at this fluence at least for 20 shots.

The change in PBD amplitude when the film is removed (Fig. 6) can be even more increased when going to higher fluences. This is demonstrated in Fig. 7, where the ablation of a photoresist film from a Cr layer was studied for four different fluences. Again, the deflection amplitude is plotted as a function of laser shots onto one spot. While the lowest fluence (0.07 J cm^{-2}) does not accomplish any ablation, the step-like changes of the shock wave signal signify film removal for higher fluences. With increasing fluence fewer laser shots are needed for ablation and the change in deflection amplitude becomes larger. For 0.54 J cm^{-2}, we noticed within three shots a factor of 9 difference in signal size between photoresist and Cr film. More re-
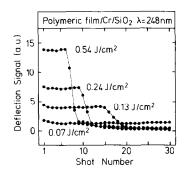

Fig. 7. Ablation of a photoresist film on a Cr layer with four different fluences in multishot mode. The PBD amplitudes are plotted versus number of laser shots on one spot. All fluences are below the ablation threshold of the Cr film.

sults of this nature have been obtained for multilayer structures, some of which are published elsewhere [17]. These data prove that the PBD technique does have the sensitivity for in-situ control of selective film removal. Note that in favorable cases incubation effects [18] can be exploited when the absorbance of film and substrate are comparable.

3.2. Dielectric coatings

One of the key issues for optical coatings is their durability under high intensity laser irradiation [2]. The PBD technique can be employed to gain in situ information about the development of damage. It is more direct and should have a greater sensitivity than microscopic inspection, which is generally used to determine damage thresholds of optical coatings. Via the slope of the deflection amplitude above the damage threshold, PBD even reveals to a certain extent information about the nature of the damage process [11, 19]. It can, for example, distinguish between dielectric breakdown and thermal evaporation. We also refer to Ref. [6] where it is shown that the slope of the data differs significantly when the photon energy is smaller or larger than the band gap of the dielectric material.

The damage resistance of optical coatings depends on the quality of the coating and its chemical composition. The latter point is demonstrated in Fig. 8. In the upper frame the fluence dependence of the PBD amplitude for a pure substrate surface is compared with one obtained with a MgF_2 coating. There is no difference in the onset of damage, and we conclude that this particular fluoride layer does not alter the damage resistivity of the substrate material at this wavelength. Most likely this is due to the large band gap of the coating material compared with the photon energy of 5 eV (248 nm) and should also prove correct for other fluorides. In contrast, adding an Al_2O_3 coating leads to a significant reduction of the damage threshold, as displayed in the lower frame of Fig. 8. We content ourselves here with showing this effect. A physical interpretation of the
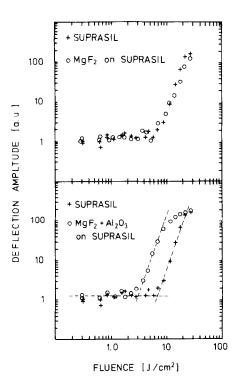
Fig. 8. The influence of optical coatings on laser damage thresholds. The upper frame shows that for 248 nm a MgF_2 coating does not affect the damage threshold of the pure suprasil (fused silica) substrate. When an Al_2O_3 coating is added, the damage threshold drops by more than a factor of two (lower frame).

threshold reduction would require a more systematic study of oxide coatings [6].

3.3. Metal films

Metal films on glass substrates are model substances for studying ablation of strongly absorbing thin films. Their optical penetration depth α^{-1} is typically 1/20 of the wavelength, they are good thermal conductors, and they usually ablate by melting and evaporation. For non-refractory metals the ablation process is well understood and the threshold fluence for vaporization can be quantitatively predicted from reflectivity and thermal properties of the material [15]. By studying the thickness dependence of the ablation threshold it was shown that a critical energy density $\varepsilon_T = F_T/L_{th}$ exists which must be overcome to accomplish ablation. Here, F_T is the threshold fluence, $L_{th} = (2\kappa\tau)^{1/2}$ the thermal diffusion length, κ the thermal diffusivity and τ the laser pulse length. For nanosecond pulses L_{th} is much larger than α^{-1}, and the heat penetrates during the pulse $L_{th}\alpha$ times deeper into the material than the laser light. The critical energy density ε_T is a constant for each film material. Consequently, when the volume decreases with thickness in the range $d < L_{th}$, the threshold fluence must be correspondingly smaller.

The following model was developed [15] to describe melting and evaporation thresholds of metal films. The

rapid heat spread during the laser pulse leads to a uniform temperature rise

$$\Delta T = \Delta Q / C_p \tag{1}$$

in a volume defined by the irradiated area and the thermal diffusion length. Here, ΔQ is the absorbed energy and C_p the heat capacity at constant pressure. For thin metal films on poor thermal conductors, such as glass, the film thickness d rather than L_{th} is the limiting factor. Eq. (1) leads to the following predictions for the threshold fluence [15]:

$$F_T^{\lessgtr} = A\left\{\left[\rho_f c_f - \frac{L_{th,s}}{L_{th,f}}\rho_s c_s\right]d + L_{th,s}\rho_s c_s\right\} \quad \text{for } d \leqslant L_{th,f} \tag{2a}$$

$$F_T^{\gtrless} = A\rho_f c_f L_{th,f} \qquad \text{for } d \geqslant L_{th,f} \tag{2b}$$

and

$$A = \frac{\Delta T}{(1 - e^{-\alpha d})(1 - R)}$$

Here, R is the reflectivity, ρ the density and c the specific heat of film (subscript f) and substrate (subscript s), respectively. The heat loss to the substrate has been taken into account additively. These relations predict both the fluence threshold for melting and that for boiling, provided the proper ΔT is used: for melting, the melting temperature; for evaporation, the vaporization temperature plus the latent heat for melting divided by $\rho_f c_f$ [15]. From Eq. (2a) we see that for $d \leqslant L_{th,f}$ the threshold fluences increase linearly with film thickness up to the point where $d = L_{th,f}$. Beyond that the threshold fluence becomes independent of thickness (Eq. (2b)) and should be equal to the value for bulk material.

These conclusions were based on systematic studies of the ablation behavior of Ni and Au films on fused silica substrates, using 248 nm, 14 ns laser pulses [15]. The quality of the underlying data is exemplified in Fig. 9, which illustrates for a 220 nm Ni film the dependence of both amplitude and transit time of the PBD signal on fluence. Threshold fluences were collected from both types of data and checked for consistency. The amplitude dependence reveals two fluence ranges, a thermal one with a linear increase of the signal with fluence, and the highly non-linear increase above F_T where the plasma develops. The melting point is near the arrow and identified by the occurence of visible marks on the surface (see also Fig. 12). Note that the transit time remains constant in the thermal range, testifying that here the signal originates from a sonic wave generated by the heated surface [16].

All threshold fluences for Ni films, extracted from data like those shown in Fig. 9, are summarized in Fig. 10 for various thicknesses. Circles represent F_T values, triangles those fluences where the irradiated spots be-
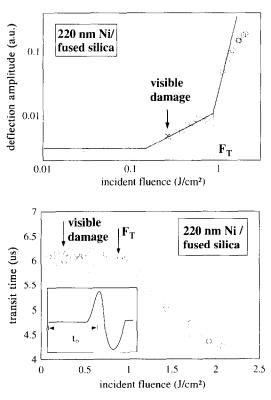
Fig. 9. Typical fluence dependence of deflection amplitude (top) and transit time (bottom) for single-shot ablation ablation (1-on-1) of a 220 nm Ni film on fused silica with 248 nm, 14 ns laser puses. The threshold for evaporation and plasma formation is denoted by F_T, the arrows mark the appearance of visible surface damage.

Fig. 10. Thickness dependence of threshold fluences for single-shot ablation (○) and melting (△) of Ni films on fused silica with 248 nm, 14 ns laser pulses. Solid and dashed-dotted lines are calculated by Eqs. (2a) and (2b) without any free parameters. Reflectivity and specific heat values used in the calculations are listed in the figure.

Fig. 11. Thickness dependence of threshold fluences for single-shot irradiation of Cr films on fused silica with 248 nm, 14 ns laser pulses. ◇, plasma thresholds obtained from transit time data; ●, amplitude thresholds which indicate the onset of film cracking; ■, occurence of visible damage. The solid and dashed-dotted lines are calculated by Eqs. (2a) and (2b), using a reflectivity $R = 0.54$ and a thermal diffusivity of 0.20 cm^2 s^{-1}.

come visible (arrows in Fig. 9). The solid and dashed-dotted lines are predictions of Eqs. (2a) and (2b), calculated with bulk material constants of Ni. For the specific heat, the mean value between room temperature and the respective melting or boiling temperature was taken. The reflectivity used is given in the inset. The thermal diffusivity was measured for all films by the transient thermal grating technique [15]. The results for the various film thicknesses agreed within their limits of error, and an average value of $\kappa = 0.19 \pm 0.02$ cm^2 s^{-1}, close to the bulk value of Ni, was adopted.

There is surprisingly good agreement between the experimental data in Fig. 10 and the predictions of this simple model, in view of the fact that there are no free parameters entering the calculations. As predicted by theory, we recognize the sharp break of the data trend at $d = L_{th}$, preceded by a linear increase of the threshold fluence with film thickness. For larger thicknesses, no further increase of threshold fluence occurs. The slope of the linear increase defines the critical energy density ε_T necessary for ablation. We want to emphasize that, without using any model, the slopes of the data below L_{th} yield, when corrected for reflectivity losses, energy densities that are close to the melting and vaporization enthalpies of bulk Ni [15]. The important conclusion is that ablation thresholds of soft metal films like Ni and
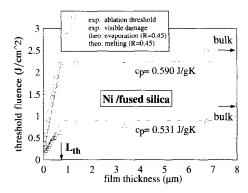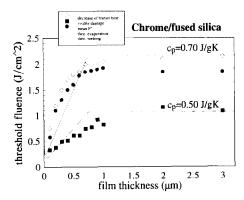
Au are predictable, both by the vaporization enthalpy of the material or the use of Eqs. (2a) and (2b).

The last statement may not pertain to films of refractory metals. To investigate this question, we studied the damage behavior of Cr films, which is of interest for applications. The results for the three thresholds (visibility, change in transit time, and increase in signal amplitude) are summarized in Fig. 11. The general trend seen for Ni films in Fig. 10 is still preserved: for small thicknesses the ablation threshold increases rapidly to reach a constant value for $d \geqslant 1$ µm. There are significant deviations, however. The rise for small film thicknesses is faster than the thermal model predicts and no sharp break at $d = L_{th,f}$ is observed. All in all the results disagree with the predictions of Eqs. (2a) and (2b), represented by solid and dashed-dotted lines. Variation of the parameters within tolerable limits does not improve this disagreement. Apparently the ansatz in Eq. (1) is too simple for Cr and there are other effects that must be included. A hint comes from the fact that in

425 nm nickel on fused silica

0.59 J/cm²   1.62 J/cm²   2.46 J/cm² |————| 50 µm

200 nm chrome on fused silica

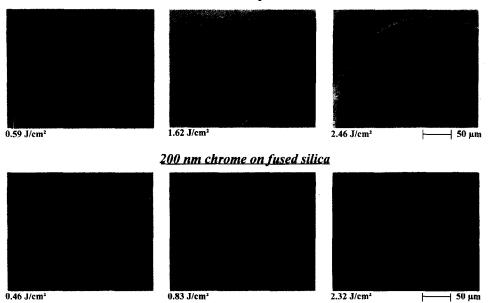0.46 J/cm²   0.83 J/cm²   2.32 J/cm² |————| 50 µm

Fig. 12. Optical images of single-shot irradiation spots on 425 nm Ni and 200 nm Cr films, imprinted by 248 nm, 14 ns laser pulses. The three pictures for each film represent the effect of the different fluences listed (cf. Figs. 10 and 11). For discussion see text.

Fig. 11 transit times yield consistently higher threshold values than amplitude signals. The break in transit time (compare Figs. 5 and 9) is due to shock waves and therefore a reliable sign of plasma expansion, which can only take place when metal is vaporized. The PBD amplitude, however, is sensitive to sound waves of any origin, i.e. also cracking sounds. The data in Fig. 11 indicate that strong sound amplitudes arising from cracking occur for all film thicknesses at fluences lower than the plasma threshold.

Microscopic images of irradiated spots on a 200 nm Cr film on fused silica support this conjecture. Fig. 12 compares the surface images of three spots on Ni and Cr films, where each spot was irradiated by one pulse of the fluence listed. For the Ni film, a fluence of 0.59 J cm^{-2} accomplishes superficial melting, leaving the resolidified surface crumpled. At 1.62 J cm^{-2} the film is molten all the way to the substrate and the surface tension of the liquid leads to formation of islands, as seen in the picture. Finally, with 2.46 J cm^{-2} the 425 nm Ni film is completely ablated and the sharp boundary reflects the top hat profile of the laser beam. The Cr film shows a distinctly different reaction to the laser pulses which is governed by film fracture. Even when the film is completely ablated for 2.32 J cm^{-2}, residual cracks are still visible in the edge region. The otherwise clean ablation at this high fluence suggests that the film was molten and evaporated [20], and yet, for the two lower fluences there is no indication of melting. It is also surprising that the cracks are larger and more abundant for the lower fluence 0.46 J cm^{-2}, as compared to those observed for 0.83 J cm^{-2}. This may suggest some annealing or perhaps even melting

process for intermediate fluences. More studies are necessary to elucidate in detail the mechanism of Cr film ablation. We noticed even stronger cracking effects for Ti films and therefore expect that film fracture is characteristic for refractory metal films.

The information gained from Fig. 12 proves that the difference between amplitude and transit time of the PBD signal for Cr films in Fig. 11 is indeed due to sound waves caused by mechanical cracking. Also, the steeper rise of the fluence threshold for ablation in Fig. 11 in comparison to the prediction of the thermal model based on Eq. (1) can be qualitatively understood. For Cr films, the critical energy density discussed above, $\varepsilon_T = F_T/L_{th}$, is composed of the vaporization enthalpy plus the additional energy it takes for fracturing the film, and hence requires higher fluences, as observed in Fig. 11. However, a more advanced model is required for a quantitative description of this non-thermal energy, involving the thermoelastic properties of the film material and its adhesion to the substrate.

4. Conclusion

In this contribution, we have demonstrated how to utilize the PBD technique for controlling laser ablation of thin films and the onset of optical damage. It was shown that this technique has the potential to distinguish between sonic and supersonic waves and is therefore sensitive to heating, cracking, evaporation, and, for dielectrics, discharge at or near the surface. The PBD technique can be applied in situ as long as there is optical access. It requires, however, a surrounding gas

for the propagation of the acoustic waves. The plasma wave was found to be irreproducible and therefore not suitable for quantitative measurements

The influence of optical coatings on the damage threshold was illustrated for a fluoride and an oxide coating. Examples were presented for the ablation of polymer and metal films with 248 nm, 14 ns laser pulses, mostly by single-shot irradiation. By measuring threshold fluences for melting and ablation as a function of film thickness, the PBD technique was able to uncover different responses of Ni and Cr films on fused silica to single-shot irradiation, which was also confirmed by microscopic inspection. Ni films melt and evaporate, while Cr films fracture before vaporizing. Melting and ablation of Ni films can be described well by a simple thermodynamic model. For Cr films, this model also reproduces the general trend with thickness of the ablation fluence, but it disagrees with the data in detail since the energy necessary to crack the films is not included.

Acknowledgements

References

[1] I.W. Boyd, *Laser Processing of Thin Films and Microstructures*, Springer Ser. Mater. Sci. Vol. 3, Springer, Berlin, Heidelberg, 1987.

[2] R.M. Wood (ed.), *Laser Damage in Optical Materials*, Adam Hilger, Bristol, 1986.

[3] E. Fogarassy and S. Lazare (eds.), *Laser Ablation of Electronic Materials*, Elsevier, Amsterdam, 1992.

[4] B. Braren, J.J. Dubowski, and D.P. Norton (eds.), *Laser Ablation in Materials Processing: Fundamentals and Applications*, Mat. Res. Soc. Symp. Proc. Vol. 285, Materials Research Society, Pittsburgh, 1993.

[5] J.C. Miller and D.B. Geohegan (eds.), *Laser Ablation: Mechanisms and Applications-II*, AIP Conf. Proc. No. 288. AIP Press. New York, 1994.

[6] M. Reichling, J. Siegel and E. Matthias, *Thin Solid Films*, *253* (1994) 333.

[7] H. Kim, J.C. Postlewaite, T. Zyung and D.D. Dlott, *J. Appl. Phys.*, *64* (1988) 2955; T. Zyung, H. Kim, J.C. Postlewaite and D.D. Dlott, *J. Appl. Phys.*, *65* (1989) 4548.

[8] R. Srinivasan, K.G. Casey, B. Braren and M. Yeh, *J. Appl. Phys.*, *67* (1990) 1604; R. Srinivasan, B.Braren and K.G. Casey, *J. Appl. Phys.*, *68* (1990) 1842.

[9] P.L.G. Ventzek, R.M. Gilgenbach, C.H. Ching and R.A. Lindley, *J. Appl. Phys.*, *72* (1992) 1696.

[10] G. Koren, *Appl. Phys. Lett.*, *51* (1987) 569.

[11] S. Petzoldt, A.P. Elg, M. Reichling, J.Reif and E. Matthias, *Appl. Phys. Lett.*, *53* (1988) 2005.

[12] J.A. Sell, D.M. Heffelfinger, P. Ventzek and R.M. Gilgenbach, *Appl. Phys. Lett.*, *55* (1989) 2435; *J. Appl. Phys.*, *69* (1991) 1330.

[13] G. Petrocelli, F. Scudieri and S. Martellucci, *Appl. Phys. B*, *52* (1991) 123.

[14] J. Diaci and J. Mozina, *Appl. Surf. Sci.*, *69* (1993) 321.

[15] E. Matthias, M. Reichling, J. Siegel, O.W. Käding, S. Petzoldt, H. Skurk, P. Bizenberger and E. Neske, *Appl. Phys. A*, *58* (1994) 129; pp. 305–320 in Ref. [5].

[16] A. Rosencwaig, *Photoacoustics and Photoacoustic Spectroscopy*, Wiley, New York, 1980, Chapter 9.

[17] E. Hunger, H. Pietsch, S. Petzoldt and E. Matthias, *Appl. Surf. Sci.*, *54* (1992) 227; E. Hunger, S. Petzoldt, H. Pietsch, J. Reif and E. Matthias, *Proc. SPIE*, *1441* (1990) 283.

[18] E. Sutcliffe and R. Srinivasan, *J. Appl. Phys.*, *60* (1986) 3315; S.Küper and M. Stuke, *Appl. Phys. A*, *49* (1989) 211; E. Matthias and Z.L. Wu, *Appl. Phys. A*, *56* (1993) 95.

[19] J. Reif, S. Petzoldt, A.P. Elg and E. Matthias, *Appl. Phys. A*, *49* (1989) 199.

[20] Z. Tóth, J. Solis, C.N. Afonso, F. Vega and T. Szörényi, *Appl. Surf. Sci.*, *69* (1993) 330.